Higher-Order Topological Corner States Induced by Gain and Loss

Xi-Wang Luo and Chuanwei Zhang

Phys. Rev. Lett. **123**, 073601 — Published 13 August 2019

DOI: 10.1103/PhysRevLett.123.073601

Higher-order topological corner states induced by gain and loss

Xi-Wang Luo and Chuanwei Zhang*
Department of Physics, The University of Texas at Dallas, Richardson, Texas 75080-3021, USA

Higher-order topological insulators and superconductors are topological phases that exhibit novel boundary states on corners or hinges. Recent experimental advances in controlling dissipation such as gain/loss in atomic and optical systems provide a powerful tool for exploring non-Hermitian topological phases. Here we show that higher-order topological corner states can emerge by introducing staggered on-site gain/loss to a Hermitian system in a trivial phase. For such a non-Hermitian system, we establish a general bulk-corner correspondence by developing a biorthogonal nested-Wilson-loop and edge-polarization theory, which can be applied to a wide class of non-Hermitian systems with higher-order topological orders. The theory gives rise to topological invariants characterizing the non-Hermitian topological multipole moments (i.e., corner states) that are protected by reflection or chiral symmetry. Such gain/loss induced higher-order topological corner states can be experimentally realized using photons in coupled cavities or cold atoms in optical lattices.

Introduction.— Topological states of matter [1–5] have been widely studied in various systems ranging from solid-state [6–8], over cold atomic [9–17] to photonic [18–24] and acoustic [25–30] systems. The states are indexed by the bulk topological invariants that determine the boundary physics with lower dimensions. Recently, the concept has been generalized to higher-order topological insulators or superconductors with novel boundary states on corners or hinges [31–50]. Different from conventional first-order topological states, the d-dimensional n-th order topological states can host $(d-n)$-dimensional gapless boundary states. The experimental realizations of such interesting higher-order topological states in photonic [37–40] and electrical circuit [41, 42] systems further enlighten the research of these novel topological matters.

Meanwhile, the search for topological states of matter has also turned to open quantum systems characterized by non-Hermitian Hamiltonians [51], which exhibit a rich variety of unique properties without Hermitian counterparts [52]. States modeled by non-Hermitian Hamiltonians appear in systems such as photonic structures with loss or gain [53–64], and cold atomic systems or solid-state materials with finite (quasi-)particle lifetime [65–72]. The eigenvalues are generally complex, and the right and left eigenstates, satisfying biorthonormolity constrains, are no longer equivalent to each other (neither of them form an orthogonal basis). Moreover, more than one right eigenstates can coalesce at exceptional points [70]. Such unique properties lead to a rich variety of interesting topological phenomena (e.g., the non-Hermitian skin effects, exceptional rings, bulk fermi arcs, etc.), with bulk-boundary correspondence very different from the Hermitian systems [73–91].

The effects of non-Hermiticity on higher-order topological physics have been considered recently in a few works [92–96], where the non-Hermiticity is induced by asymmetric tunnelings, leading to the observation of interesting phenomena such as higher-order skin effect [92] and biorthogonal bulk polarization [96]. Nevertheless, a general bulk-corner correspondence of the non-Hermitian higher-order topological states is still elusive. In addition, compared to asymmetric tunnelings, a simpler and more tunable way for introducing non-Hermiticity in photonic and atomic experiments is to control the on-site particle dissipations directly. Therefore two natural questions arise: *i*) Can higher-order topological states be induced by simply controlling the on-site gain or loss? *ii*) Is there a general bulk-corner correspondence for the non-Hermitian higher-order topological states?

In this Letter, we address these two important questions by considering a 2-dimensional (2D) lattice model with staggered on-site particle gain/loss. Our main results are:

i) The non-Hermitian particle gain and loss can drive the system from a trivial phase to a second-order topological phase with the emergence of four degenerate corner states.

ii) We develop the biorthogonal nested-Wilson-loop and edge-polarization approach which gives rise to bulk topological invariants responsible for the gapless corner states. The topological invariants are protected by reflection or chiral symmetries. In the presence of additional C_4 rotation symmetry, the topology can also be characterized by a quantized biorthogonal winding number.

iii) Although we focus on 2D reflection-symmetric case, our model and the bulk-corner correspondence can be generalized to study d-dimensional d-th order non-Hermitian topological states with either reflection or chiral symmetries.

iv) Simple experimental schemes based on photons in coupled cavities and cold atoms in optical lattices are proposed. Our system only relies on the manipulation of on-site particle gain/loss, and is ready for experimental exploration.

The model.— We consider a 2D lattice model with staggered tunnelings along both horizontal and vertical directions, as shown in Fig. 1(a). There is an effective magnetic flux $\phi = \pi$ for each plaquette, which appears as the tunneling phases on the dashed lines. The non-Hermiticity is introduced by the particle loss (gain) on all

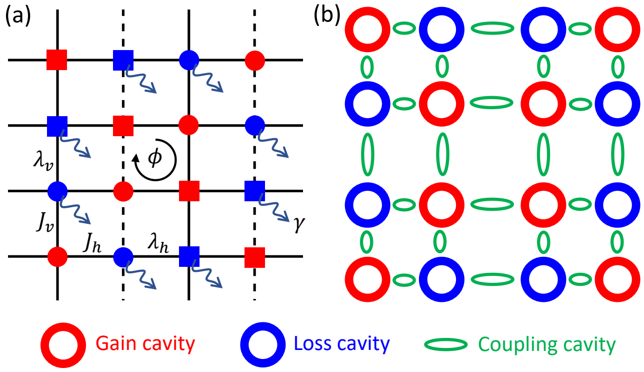

FIG. 1: (a) Lattice representation of the non-Hermitian model in Eq. 1. All sites in blue (red) have particle loss (gain) with a rate γ. ϕ is the magnetic flux for each plaquette, and $J_{h,v}$ ($\lambda_{h,v}$) are the tunneling amplitudes between sites in different color (shape) along the horizontal and vertical directions, respectively. (b) Experimental implementation of the lattice model in (a) using coupled arrays of micro-ring cavities.

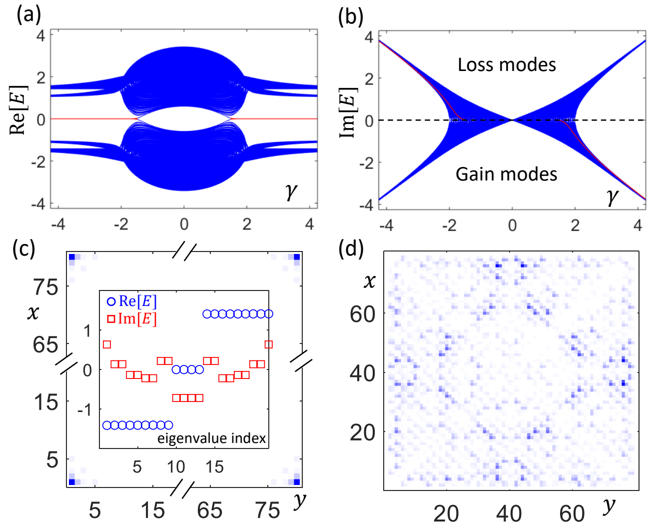

FIG. 2: (a) (b) Energy spectra of the non-Hermitian Hamiltonian Eq. 1 with open boundaries in both directions. The bulk energy gap closes at $|\gamma| = \gamma_c$, where a topological phase transition occurs and in-gap corner states (red curves with four-fold degeneracy) emerge at $|\gamma| > \gamma_c$. (c) Typical density distributions $|\Psi^R_{\rm corner}(x,y)|^2$ of the four corner states, with $|\Psi^R_{\rm corner}(x,y)\rangle$ the right eigenstate. The inset shows the corresponding eigenenergies around the four corner states with $\mathrm{Re}[E] = 0$. (d) Typical density distributions of the bulk states. $\gamma = 2$ in (c) and (d). Common parameters: system size $N_h = N_v = 20$ (unit cells), $J = \sqrt{2}$ and $\lambda_v = 1$ (leading to $\gamma_c = \sqrt{2}$). We set $\lambda_h = 1$ as energy unit.

blue (red) lattice sites. We choose 16 orbitals in Fig. 1(a) as our unit cell with horizontal and vertical primitive-lattice vectors. The Hamiltonian reads

$$\begin{aligned} H(\mathbf{k}) \;=\; & J_h\sigma_h^x + J_v\sigma_v^x\sigma_h^\phi + i\gamma\sigma_h^z\sigma_v^z\tau_h^z\tau_v^z \\ & +\lambda_h(\tau_h^-\sigma_h^+ + e^{-ik_x}\tau_h^-\sigma_h^- + h.c.) \\ & +\lambda_v\sigma_h^\phi(\tau_v^-\sigma_v^+ + e^{-ik_y}\tau_v^-\sigma_v^- + h.c.), \end{aligned} \quad (1)$$

where $J_{h,v} > 0$ ($\lambda_{h,v} > 0$) are the nearest-neighbour tunneling amplitudes between red and blue (circle and square) sites, $\sigma_{h,v}$ ($\tau_{h,v}$) are the Pauli matrices for the degrees of freedom spanned by red and blue (circle and square) sites, and h, v represent the horizontal and vertical directions, respectively. $\sigma^\phi_{h,v} = \sigma^z_{h,v}$ for $\phi = \pi$. The gain/loss rate γ in Eq. 1 is positive since the blue sites are lossy. Alternatively, we may consider a different gain/loss configuration with gain (loss) on blue (red) sites, which simply changes γ to negative. In experiments, the Hamiltonian can be realized using cold atoms in optical lattices or photons in coupled cavities [97]. Fig. 1 (b) is an example based on arrays of coupled micro-ring cavities, where the coupling amplitude and phase between neighbour cavities, and the photon gain/loss for each cavity can be controlled independently [40, 61].

Corner states.— For simplicity, we assume $J_h = J_v \equiv J$ throughout this paper, and the physics for $J_h \neq J_v$ is similar. The system has 16 bands [97], which appear in pairs $E(\mathbf{k}) = -E^*(\mathbf{k})$ due to the pseudo-anti-Hermiticity $\eta H \eta = -H^\dagger$ with $\eta = \sigma_h^z\sigma_v^z\tau_h^z\tau_v^z$. We are interested in the half-filling gap around $\mathrm{Re}[E] = 0$. We focus on the region $\lambda_{h(v)} \leq J$ (the system stays in the trivial insulating/metal phase at the Hermitian limit $\gamma = 0$ [31, 32]), and show that the second-order topological corner states can be induced solely by non-Hermitian gain and loss.

In Figs. 2(a) and (b), we plot the energy spectrum as a function of γ, with open boundaries along both directions. Effectively, the particle loss reduces the tunnelings between gain and loss sites, while the tunnelings between two loss (gain) sites are not affected. We see that as $|\gamma|$ increases, the bulk gap closes and reopens (the small derivation is the finite size effect) at a critical point γ_c, leading to a topological phase transition with the emergency of four in-gap states. The typical density distributions of these in-gap states are shown in Fig. 2(c), which are well localized at four corners. We emphasize that our system does not suffer from the non-Hermitian skin effects due to the trivial eigenenergy vorticity [80] $\oint \partial_{\mathbf{k}}\mathrm{Arg}[E(\mathbf{k})]d\mathbf{k} = 0$ for any loop in the momentum space, therefore it does not matter whether the right or/and left eigenstates are used to calculate the density distribution. As a result, the bulk states of $H(\mathbf{k})$ do distribute in the bulk [see Fig. 2(d)], and the open-boundary bulk spectrum is the same as that for periodic boundaries. We set $\lambda_h = \lambda_v$ in Fig. 2, therefore the system undergoes a bulk gap closing across the topological phase transition due to the C_4 symmetry [45]. In general, the second-order topology can be altered by the gap closing in either the bulk or edge spectrum, and the emergency of corner states does not require bulk energy gap closing for $\lambda_h \neq \lambda_v$ [32, 45], which will be further illustrated.

Topological invariants.— For Hermitian systems, it was shown that the topology of the nested Wilson loop and edge polarization are responsible for the corner states [31, 32]. Here we develop their non-Hermitian counterparts and show that the non-Hermitian corner states are originated from the topology of the generalized biorthogonal nested Wilson loops and edge polarizations. We consider a general Hamiltonian $H(\mathbf{k})$ on a torus with periodic boundaries and define the biorthogonal Wilson loop operator as

$$W_{h,\mathbf{k}} = \mathcal{P}\exp[i\int_{k_x}^{k_x+2\pi} A_h(k_x', k_y)dk_x'], \tag{2}$$

where $A_h(\mathbf{k}) = -i\langle u_{n,\mathbf{k}}^L|\partial_{k_x}|u_{m,\mathbf{k}}^R\rangle$ is the biorthogonal non-Abelian Berry connection in the horizontal direction, $|u_{m,\mathbf{k}}^{R,L}\rangle$ are the m-th occupied right and left Bloch eigenstates satisfying $H(\mathbf{k})|u_{m,\mathbf{k}}^R\rangle = E_m(\mathbf{k})|u_{m,\mathbf{k}}^R\rangle$, $H^\dagger(\mathbf{k})|u_{m,\mathbf{k}}^L\rangle = E_m^*(\mathbf{k})|u_{m,\mathbf{k}}^L\rangle$ and $\langle u_{n,\mathbf{k}}^L|u_{m,\mathbf{k}}^R\rangle = \delta_{n,m}$, and $\mathcal{P}$ is the path-ordering operator. Different from the Hermitian case [31], $W_{h,\mathbf{k}}$ may no longer be a unitary operator, and leads to a non-Hermitian Wannier Hamiltonian $H_{W_h}(\mathbf{k}) = -\frac{i}{2\pi}\log W_{h,\mathbf{k}}$, which also has different left and right eigenstates, that is, $H_{W_h}(\mathbf{k})|\varepsilon_{h,j,\mathbf{k}}^R\rangle = \varepsilon_{h,j,k_y}|\varepsilon_{h,j,\mathbf{k}}^R\rangle$, $H_{W_h}^\dagger(\mathbf{k})|\varepsilon_{h,j,\mathbf{k}}^L\rangle = \varepsilon_{h,j,k_y}^*|\varepsilon_{h,j,\mathbf{k}}^L\rangle$ with $\langle\varepsilon_{h,j,\mathbf{k}}^L|\varepsilon_{h,j',\mathbf{k}}^R\rangle = \delta_{j,j'}$ and j the Wannier band index. The non-Hermitian Wannier bands (independent from k_x), which obey the identification $\mathrm{Re}[\varepsilon_{h,j,k_y}] \equiv \mathrm{Re}[\varepsilon_{h,j,k_y}]$ mod 1, can carry topological invariants if they are gapped.

The biorthogonal vertical polarization for the Wannier band sector ε_h can be defined as

$$p_v^{\varepsilon_h} = -\frac{i}{4\pi^2}\int dk_x \log\det[\tilde{W}_{h,\mathbf{k}}]. \tag{3}$$

Here $\tilde{W}_{h,\mathbf{k}}$ is the biorthogonal nested Wilson loop along the vertical direction, which is defined on the Wannier sector ε_h with non-Hermitian Wannier-band basis $|w_{h,j,\mathbf{k}}^{R(L)}\rangle = \sum_{m=1}^{N_{\mathrm{occ}}}|u_{m,\mathbf{k}}^{R(L)}\rangle[|\varepsilon_{h,j,\mathbf{k}}^{R(L)}\rangle]_m$ (N_{occ} is the number of occupied energy bands and $\langle w_{h,j,\mathbf{k}}^L|w_{h,j',\mathbf{k}}^R\rangle = \delta_{j,j'}$) [97]. Similarly, we can obtain the biorthogonal nested Wilson loop along the horizontal direction and the corresponding polarization $p_h^{\varepsilon_v}$. There would be corner states when $p_{h,v}^{\varepsilon_{v,h}}$ are non-trivial.

On the other hand, even for trivial $p_{h,v}^{\varepsilon_{v,h}}$, one may still have corner states if the edge polarization is non-trivial [32]. For non-Hermitian systems, we should use the biorthogonal edge polarization, which are obtained by considering a cylindrical geometry and calculating the pseudo-one-dimensional biorthogonal Wannier values ($\varepsilon_{h,j}$ or $\varepsilon_{v,j}$) and polarization ($p_h^{i_v}$ or $p_v^{i_h}$ with i_v or i_h the unit-cell index along the open direction) along the periodic direction (horizontal or vertical) [97]. The second-order corner modes are characterized by the vanishing bulk polarization (*i.e.*, $i_{v,h}$ away from 1 and $N_{v,h}$), but quantized non-zero edge-localized polarization p_h^{edge} and/or p_v^{edge} (*i.e.*, $i_{v,h}$ near 1 or $N_{v,h}$) [97].

In general, higher-order topological phases are protected by symmetries [31, 32]. We consider a Hamiltonian that respects either reflection symmetries $M_hH(k_x,k_y)M_h^{-1} = H(-k_x,k_y)$ and $M_vH(k_x,k_y)M_v^{-1} = H(k_x,-k_y)$, or chiral (sublattice) symmetry $\Xi H(k_x,k_y)\Xi^{-1} = -H(k_x,k_y)$, with symmetry operators given by M_h, M_v or Ξ. Since the biorthogonal Wannier bands or values (on a torus or cylinder) change the signs under reflection operation, they are either flat bands locked at 0 or $\frac{1}{2}$, or appear in $\pm\varepsilon$ pairs for reflection-symmetric systems. The reflection symmetries also ensure the quantization of ($p_h^{\varepsilon_v}$, $p_v^{\varepsilon_h}$) and (p_h^{edge}, p_v^{edge}) with value 0 or $\frac{1}{2}$. Similar properties hold for the chiral-symmetric systems with non-Hermiticity induced by asymmetric tunneling [97].

The Wannier bands correspond to the position of the particle density cloud [31, 32]. We focus on the Wannier sectors $\in (0, \frac{1}{2})$ [or $\in (\frac{1}{2}, 1)$] which are responsible for the edge topology and corner states. Based on the Wannier-sector and edge polarizations, we define two topological invariants: $Q_1 = 4p_v^{\varepsilon_h}p_h^{\varepsilon_v}$ mod 2 [with $\varepsilon_{v,h}$ the Wannier sector $\in (0, \frac{1}{2})$] and $Q_2 = 2(p_h^{\mathrm{edge}} + p_v^{\mathrm{edge}})$ mod 2. For the topological phase, we have either $Q_1 = 1$ or $Q_2 = 1$; while for the trivial phase, we have both $Q_1 = 0$ and $Q_2 = 0$. The above bulk-corner correspondence can apply to any non-Hermitian systems with reflection or chiral symmetries, and are reduced to the normal nested-Wilson-loop and edge-polarization theory [31] in the Hermitian limit.

Phase diagram.— As an example, we study the phase diagram of the model in Fig. 1 based on the biorthogonal topological invariants. The corresponding Hamiltonian satisfies reflection symmetries with $M_h = \sigma_v^\phi\sigma_h^x\tau_h^x$ and $M_v = \sigma_v^x\tau_v^x$. It also possesses the rotational symmetry $C_4H(k_x,k_y)C_4^{-1} = H(k_y,-k_x)$ if $\lambda_h = \lambda_v$, where $C_4 = C_\tau \otimes C_\sigma$ with

$$C_\tau = \frac{1}{2}\sum_{s\neq\bar{s}}\left[\tau_s^+(\frac{1-\tau_{\bar{s}}^z}{2}) + \tau_s^-(\frac{1+\tau_{\bar{s}}^z}{2})\right], \tag{4}$$

and C_σ has a similar expression with $s, \bar{s} = \{h, v\}$. In Fig. 3(a), we show the phase diagram in the γ-λ_v plane with $J/\lambda_h = \sqrt{2}$. The phase diagram is symmetric with respect to $\gamma = 0$, so we focus on $\gamma \geq 0$. The right and left parts of the phase diagram belong to topological and trivial phases, with their boundary given by the solid line. The trivial phase enlarges with the phase boundary shifting rightward as we increase J. There are two topological phases: T-I with $(Q_1, Q_2) = (1, 0)$ and T-II with $(Q_1, Q_2) = (0, 1)$.

We first consider the C_4 symmetric case for $\lambda_v = \lambda_h$, with the open-boundary spectra shown in Fig. 2(a). The typical Wannier bands for the Hamiltonian Eq. 1 with

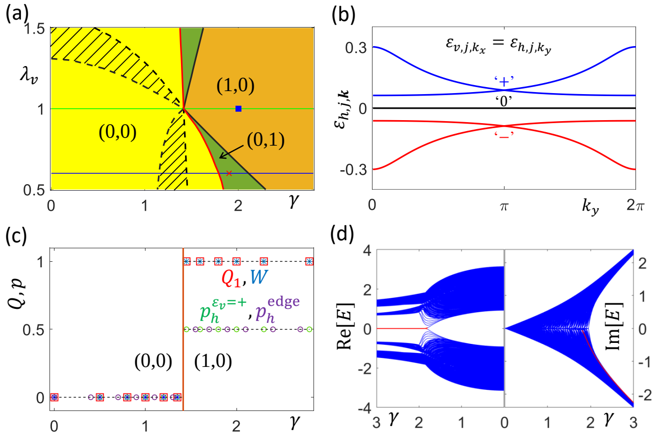

FIG. 3: (a) Phase diagram in the γ-λ_v plane for $J = \sqrt{2}\lambda_h$, with one trivial phase [yellow area with $(Q_1, Q_2) = (0, 0)$] and two topological phases [T-I: orange area with $(1, 0)$ and T-II: green area with $(0, 1)$]. The patterned region has a vanishing Wannier-band gap [97]. (b) Wannier band structures with $\lambda_v = \lambda_h$ and $\gamma = 2$ [the blue square in (a)]. The imaginary parts are locked at 0. (c) Wannier-sector (green circles) and edge (purple circles) polarizations as well as topological invariant Q_1 (red squares) and winding number W (blue stars), with $\lambda_v = \lambda_h$ [the thin green line in (a)]. (d) Complex energy spectra with open boundaries [$N_h = N_v = 20$ (unit cells)] and $\lambda_v = 0.6\lambda_h$ [the thin blue line in (a)]. The bulk gap persists upon the phase transition. We set $\lambda_h = 1$ as the energy unit.

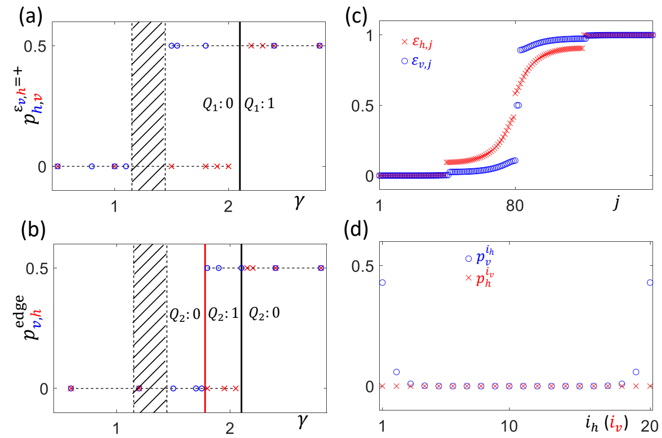

FIG. 4: (a) and (b) The horizontal (blue circles) and vertical (red crosses) polarizations for $\lambda_v = 0.6\lambda_h$ [along the thin blue line in Fig. 3(a)]. The polarization $p_h^{\varepsilon_v}$ is ill-defined in the patterned region due to the vanishing gap between Wannier sectors. The phase boundaries are given by the solid lines. (c) and (d) The Wannier values ($\varepsilon_{h,j}$, $\varepsilon_{v,j}$) and edge-polarization distributions ($p_h^{i_v}$, $p_v^{i_h}$) for the cylindrical geometry with $\lambda_v = 0.6\lambda_h$ and $\gamma = 1.9$ [indicated by the red cross in Fig. 3(a)]. Blue circles (red crosses) are the results for open boundary along horizontal (vertical) direction. The in gap Wannier values at $\frac{1}{2}$ are responsible for the edge polarization. Other parameters are the same as in Fig. 3.

periodic boundaries are shown in Fig. 3(b). There are 8 Wannier bands, with four located around $\varepsilon = 0$, two at $0 < \text{Re}[\varepsilon] < \frac{1}{2}$ and two at $0 > \text{Re}[\varepsilon] > -\frac{1}{2}$, forming three Wannier sectors labeled by $0, \pm$, as shown in Fig. 3(b). Only the '$\pm$'-Wannier sectors are responsible for the edge topology and corner states. In fact, the '0'-Wannier sector is trivial in the whole parameter space and the '$\pm$'-Wannier sectors always have the same topology. Due to the C_4 symmetry, we have $p_h^{\varepsilon_v=\pm} = p_v^{\varepsilon_h=\pm}$ and $p_h^{\text{edge}} = p_v^{\text{edge}}$, all of which jump from 0 to $\frac{1}{2}$ across the phase transition as γ increases [see Fig. 3(c)]. We would like to point out that, with C_4 symmetry, the topology can also be characterized by the biorthogonal winding number W along the high-symmetry line $k_x = k_y$ in the reflection-rotation (C_4M_h) subspace [97].

For $\lambda_v \neq \lambda_h$, the bulk energy gap persists [see Fig. 3(d)], and the phase transitions are driven by gap close/reopen in the edge spectra and the Wannier bands, which lead to polarization jumps. In the following, we focus on $\lambda_v < \lambda_h$ without loss of generality, and show how the topological invariants and phases change as we increase γ, as shown in Figs. 4(a) and (b). (i) First, the vertical Wannier bands $\varepsilon_{v,j,\mathbf{k}}$ close the gap between '0' and '$\pm$' sectors in the patterned region in Fig. 3(a) [97]. Further increasing γ reopens the gap and leads to the the jump of $p_h^{\varepsilon_v=\pm}$ from 0 to $\frac{1}{2}$. (ii) Then, the gap for the edge spectra closes and reopens on the red solid line, where p_v^{edge} jumps from 0 to $\frac{1}{2}$ and the system enters the T-II phase with the emergence of corner states. Shown in Figs. 4(c) and (d) are the Wannier values ($\varepsilon_{h,j}$ and $\varepsilon_{v,j}$) and edge-polarization distribution ($p_h^{i_v}$ and $p_v^{i_h}$) for the phase T-II on a cylinder. (iii) Finally, $\varepsilon_{h,j,\mathbf{k}}$ close the gap between '+' and '−' sectors on the black solid line, where both $p_v^{\varepsilon_h=\pm}$ and p_h^{edge} jump from 0 to $\frac{1}{2}$, and we reach the T-I phase. Both T-I and T-II phases support corner states, and they are distinguished by the edge topology [97]. The T-II phase region shrinks to zero as λ_v approaches λ_h, where all edge and Wannier-sector polarizations jump at the same γ due to the C_4 symmetry. These phenomena are very different from the Hermitian case. Especially, one can only have the topological phase T-I for the Hermitian limit, where all edge polarizations must vanish as long as $Q_1 = 0$ [32]. The appearance of phase T-II is a result of the interplay between the non-Hermiticity and the C_4 symmetry breaking [97].

Discussions.— It is possible to generalize our study by considering different flux configurations. As a simple example, one may consider $\phi = 0$ and set $\sigma_{h,v}^{\phi} = \sigma_{h,v}^{0}$ in the Hamiltonian Eq. 1. For such a zero flux model, the Hermitian part is a gapless metal when $|\lambda_h - \lambda_v| \leq 2J$. The gain/loss term effectively reduces the tunneling J and can open a topological gap with in-gap corner states [97]. Moreover, it is straightforward to generalize our non-Hermitian model and bulk-corner correspondence to higher-dimensional systems (e.g., 3D system supporting third-order topological phases with quantized octupole moment) [97]. Finally, we consider a general asymmetric-tunneling model (without on-site gain/loss) as an example of chiral symmetric systems, and confirm the bulk-corner correspondence numerically [97]. The asymmetric tunnelings break both the Hermiticity and reflection symmetries (other symmetries like C_4 rotation or reflection-rotation C_4M_h are also broken). As we increase the strength of the non-Hermiticity (i.e., asymmetry), the system can transform from the trivial phase to the second-order topological phase with zero-energy modes at four corners, which are characterized by the non-trivial topology of the biorthogonal nested Wilson loops [97].

Conclusion.— In summary, we propose a scheme to realize non-Hermitian higher-order topological insulators by simply controlling the on-site gain or loss, and show that the non-Hermitian corner states are characterized by the bulk topology in the form of biorthogonal nested Wilson loops or edge polarizations. The generalized bulk-corner correspondence may work for a wide class of non-Hermitian d-dimensional d-order topological systems with reflection or chiral symmetries. The proposed model can be realized easily in experiments. Our work offers a tunable method for manipulating corner states through dissipation control, and paves the way for the study of various non-Hermiticity induced higher-order topological states of matter and the classifications of them.

Acknowledgements: This work is supported by AFOSR (FA9550-16-1-0387), NSF (PHY-1806227), and ARO (W911NF-17-1-0128). Part of C.Z. work was performed at the Aspen Center for Physics, which is supported by National Science Foundation grant PHY-1607611.

* Corresponding author.
Email: chuanwei.zhang@utdallas.edu

[1] D. Xiao, M.-C. Chang, and Q. Niu, Berry phase effects on electronic properties, Rev. Mod. Phys. **82**, 1959 (2010).
[2] M. Hasan and C. Kane, Colloquium: topological insulators, Rev. Mod. Phys. **82**, 3045 (2010).
[3] X.-L. Qi and S.-C. Zhang, Topological insulators and superconductors, Rev. Mod. Phys. **83**, 1057 (2011).
[4] C.-K. Chiu, J. C. Y. Teo, A. P. Schnyder, and S. Ryu, Classification of topological quantum matter with symmetries, Rev. Mod. Phys. **88**, 035005 (2016).
[5] M. Sato, and Y. Ando, Topological superconductors: a review, Rep. Prog. Phys. **80**, 076501 (2017).
[6] C. L. Kane and E. J. Mele, Z_2 Topological Order and the Quantum Spin Hall Effect, Phys. Rev. lett. **95**, 146802 (2005).
[7] B. A. Bernevig, T. L. Hughes, S.-C. Zhang, Quantum Spin Hall Effect and Topological Phase Transition in HgTe Quantum Wells, Science **314**, 1757 (2006).
[8] M. König, S. Wiedmann, C. Brüne, A. Roth, H. Buhmann, L. W. Molenkamp, X.-L. Qi, S.-C. Zhang, Quantum Spin Hall Insulator State in HgTe Quantum Wells, Science **318**, 766 (2007).
[9] M. Aidelsburger, M. Atala, M. Lohse, J. T. Barreiro, B. Paredes, and I. Bloch, Realization of the Hofstadter Hamiltonian with Ultracold Atoms in Optical Lattices, Phys. Rev. lett. **111**, 185301 (2013).
[10] H. Miyake, G. A. Siviloglou, C. J. Kennedy, W. C. Burton, and W. Ketterle, Realizing the Harper Hamiltonian with Laser-Assisted Tunneling in Optical Lattices, Phys. Rev. lett. **111**, 185302 (2013).
[11] M. Aidelsburger, M. Lohse, C. Schweizer, M. Atala, J. T. Barreiro, S. Nascimbéne, N. R. Cooper, I. Bloch, and N. Goldman, Measuring the Chern number of Hofstadter bands with ultracold bosonic atoms, Nat. Phys. **11**, 162 (2014).
[12] G. Jotzu, M. Messer, R. Desbuquois, M. Lebrat, T. Uehlinger, D. Greif, and T. Esslinger, Experimental realization of the topological Haldane model with ultracold fermions, Nature **515**, 237 (2014).
[13] N. Goldman, G. Juzeliunas, P. Ohberg, and I. B. Spielman, Light-induced gauge fields for ultracold atoms, Rep. Prog. Phys. **77**, 126401 (2014).
[14] T. Li, L. Duca, M. Reitter, F. Grusdt, E. Demler, M. Endres, M. Schleier-Smith, I. Bloch, and U. Schneider, Bloch state tomography using Wilson lines, Science **352**, 109, (2016).
[15] N. Fläschner, B. S. Rem, M. Tarnowski, D. Vogel, D.-S. Lühmann, K. Sengstock, and C. Weitenberg, Experimental reconstruction of the Berry curvature in a Floquet Bloch band, Science **352**, 1091 (2016).
[16] N. Goldman, J. C. Budich, and P. Zoller, Topological quantum matter with ultracold gases in optical lattices, Nat. Phys. **12**, 639 (2016).
[17] N. R. Cooper, J. Dalibard, I. B. Spielman, Topological Bands for Ultracold Atoms, Rev. Mod. Phys. **91**, 015005 (2019).
[18] F. D. M. Haldane, and S. Raghu, Possible Realization of Directional Optical Waveguides in Photonic Crystals with Broken Time-Reversal Symmetry, Phys. Rev. Lett. **100**, 013904 (2008).
[19] M. Hafezi, E. A. Demler, M. D. Lukin, and J. M. Taylor, Robust optical delay lines with topological protection, Nature Phys. **7**, 907 (2011).
[20] K. Fang, Z. Yu, and S. Fan, Realizing effective magnetic field for photons by controlling the phase of dynamic modulation, Nature Photon. **6**, 782 (2012).
[21] L. Lu, J. D. Joannopoulos, and M. Soljačić, Topological photonics, Nature Photon. **8**, 821 (2014).
[22] Y. E. Kraus, Y. Lahini, Z. Ringel, M. Verbin, and O. Zilberberg, Topological states and adiabatic pumping in quasicrystals, Phys. Rev. Lett. **109**, 106402 (2012).
[23] M. Hafezi, S. Mittal, J. Fan, A. Migdall and J. M. Taylor, Imaging topological edge states in silicon photonics, Nature Photon. **7**, 1001 (2013).
[24] T. Ozawa, H. M. Price, A. Amo, N. Goldman, M. Hafezi, L. Lu, M. Rechtsman, D. Schuster, J. Simon, O. Zilberberg, and I. Carusotto, Topological Photonics, Rev. Mod. Phys. **91**, 015006 (2019).
[25] Z. Yang, F. Gao, X. Shi, X. Lin, Z. Gao, Y. Chong, and B. Zhang, Topological Acoustics, Phys. Rev. Lett. **114**, 114301 (2015).
[26] M. Xiao, W.-J. Chen, W.-Y. He, and C. T. Chan, Synthetic gauge flux and Weyl points in acoustic systems, Nat. Phys. **11**, 920 (2015).
[27] C. He, X. Ni, H. Ge, X.-C. Sun, Y.-B. Chen, M.-H. Lu, X.-P. Liu, and Y.-F. Chen, Acoustic topological insulator

and robust one-way sound transport, Nat. Phys. **12**, 1124 (2016).
[28] H. He, C. Qiu, L. Ye, X. Cai, X. Fan, M. Ke, F. Zhang, and Z. Liu, Topological negative refraction of surface acoustic waves in a Weyl phononic crystal, Nature **560**, 61 (2018).
[29] J. Lu, C. Qiu, W. Deng, X. Huang, F. Li, F. Zhang, S. Chen, and Z. Liu, Valley topological phases in bilayer sonic crystals, Phys. Rev. lett. **120**, 116802 (2018).
[30] G. Ma, M. Xiao and C. T. Chan, Topological phases in acoustic and mechanical systems, Nat. Rev. Phys. **1**, 281 (2019).
[31] W. A. Benalcazar, B. A. Bernevig, and T. L. Hughes, Quantized electric multipole insulators, Science **357**, 61 (2017).
[32] W. A. Benalcazar, B. A. Bernevig, and T. L. Hughes, Electric multipole moments, topological multipole moment pumping, and chiral hinge states in crystalline insulators, Phys. Rev. B **96**, 245115 (2017).
[33] J. Langbehn, Y. Peng, L. Trifunovic, F. von Oppen, and P. W. Brouwer, Reflection-Symmetric Second-Order Topological Insulators and Superconductors, Phys. Rev. lett. **119**, 246401 (2017).
[34] Z. Song, Z. Fang, and C. Fang, $(d-2)$-Dimensional Edge States of Rotation Symmetry Protected Topological States, Phys. Rev. lett. **119**, 246402 (2017).
[35] M. Lin and T. L. Hughes, Topological quadrupolar semimetals, Phys. Rev. B **98**, 241103 (2018).
[36] F. Schindler, A. M. Cook, M. G. Vergniory, Z. Wang, S. S. P. Parkin, B. A. Bernevig, and T. Neupert, Higher-order topological insulators, Sci. Adv. **4**, eaat0346 (2018).
[37] A. Hassan, F. Kunst, A. Moritz, G. Andler, E. Bergholtz, and M. Bourennane, Corner states of light in photonic waveguides, arXiv:1812.08185 (2018).
[38] B.-Y. Xie, H.-F. Wang, H.-X. Wang, X.-Y. Zhu, J.-H. Jiang, M.-H. Lu, and Y.-F. Chen, Second-order photonic topological insulator with corner states, Phys. Rev. B **98**, 205147 (2018).
[39] M. Serra-Garcia, V. Peri, R. Süsstrunk, O. R. Bilal, T. Larsen, L. G. Villanueva, and S. D. Huber, Observation of a phononic quadrupole topological insulator, Nature **555**, 342 (2018).
[40] S. Mittal, V. Vikram Orre, G. Zhu, M. A. Gorlach, A. Poddubny, and M. Hafezi, Photonic quadrupole topological phases, arXiv:1812.09304 (2018).
[41] S. Imhof, *et. al.*, Topolectrical-circuit realization of topological corner modes, Nat. Phys. **14**, 925 (2018).
[42] C. W. Peterson, W. A. Benalcazar, T. L. Hughes and G. Bahl, A quantized microwave quadrupole insulator with topologically protected corner states, Nature **555**, 346 (2018).
[43] M. Ezawa, Higher-Order Topological Insulators and Semimetals on the Breathing Kagome and Pyrochlore Lattices, Phys. Rev. Lett. **120**, 026801 (2018).
[44] F. K. Kunst, G. van Miert, and E. J. Bergholtz, Lattice models with exactly solvable topological hinge and corner states, Phys. Rev. B **97**, 241405 (2018).
[45] M. Geier, L. Trifunovic, M. Hoskam, and P. W. Brouwer, Second-order topological insulators and superconductors with an order-two crystalline symmetry, Phys. Rev. B **97**, 205135 (2018).
[46] Q. Wang, C.-C. Liu, Y.-M. Lu, and F. Zhang, High-Temperature Majorana Corner States, Phys. Rev. Lett. **121**, 186801 (2018).
[47] Z. Yan, F. Song, and Z. Wang, Majorana Corner Modes in a High-Temperature Platform, Phys. Rev. Lett. **121**, 096803 (2018).
[48] L. Trifunovic and P. W. Brouwer, Higher-Order Bulk-Boundary Correspondence for Topological Crystalline Phases, Phys. Rev. X **9**, 011012 (2019).
[49] C.-H. Hsu, P. Stano, J. Klinovaja, and D. Loss, Majorana Kramers Pairs in Higher-Order Topological Insulators, Phys. Rev. Lett. **121**, 196801 (2018).
[50] S. A. A. Ghorashi, X. Hu, T. L. Hughes, and E. Rossi, Second-order Dirac superconductors and magnetic field induced Majorana hinge modes, arXiv:1901.07579 (2019).
[51] C. M. Bender, Making Sense of Non-Hermitian Hamiltonians, Rep. Prog. Phys. **70**, 947 (2007).
[52] V. M. Martinez Alvarez, J. E. Barrios Vargas, M. Berdakin, and L. E. F. Foa Torres, Topological states of non-Hermitian systems, Eur. Phys. J. Spec. Top. **227**, 1295 (2018).
[53] K. G. Makris, R. El-Ganainy, D. N. Christodoulides, and Z. H. Musslimani, Beam Dynamics in $\mathcal{PT}$ Symmetric Optical Lattices, Phys. Rev. Lett. **100**, 103904 (2008).
[54] A. Regensburger, C. Bersch, M.-A. Miri, G. Onishchukov, D. N. Christodoulides, and U. Peschel, Parity-time synthetic photonic lattices, Nature **488**, 167 (2012).
[55] S. Malzard, C. Poli, and H. Schomerus, Topologically Protected Defect States in Open Photonic Systems with Non-Hermitian Charge-Conjugation and Parity-Time Symmetry, Phys. Rev. Lett. **115**, 200402 (2015).
[56] Y. N. Joglekar, and A. K. Harter, Passive parity-time-symmetry-breaking transitions without exceptional points in dissipative photonic systems, Photon. Res. **6**, A51 (2018).
[57] H. Jing, S. K. Özdemir, X.-Y. Lü, J. Zhang, L. Yang, and F. Nori, $\mathcal{PT}$-Symmetric Phonon Laser, Phys. Rev. Lett. **113**, 053604 (2014).
[58] B. Peng, Ş. K. Özdemir, S. Rotter, H. Yilmaz, M. Liertzer, F. Monifi, C. M. Bender, F. Nori, and L. Yang, Loss-induced suppression and revival of lasing, Science **346**, 328 (2014).
[59] J. M. Zeuner, M. C. Rechtsman, Y. Plotnik, Y. Lumer, S. Nolte, M. S. Rudner, M. Segev, and A. Szameit, Observation of a Topological Transition in the Bulk of a Non-Hermitian System, Phys. Rev. Lett. **115**, 040402 (2015).
[60] S. Weimann, M. Kremer, Y. Plotnik, Y. Lumer, S. Nolte, K. G. Makris, M. Segev, M. C. Rechtsman, and A. Szameit, Topologically protected bound states in photonic parity-time-symmetric crystals, Nat. Mater. **16**, 433 (2017).
[61] H. Zhao, P. Miao, M. H. Teimourpour, S. Malzard, R. El-Ganainy, H. Schomerus, and L. Feng, Topological hybrid silicon microlasers, Nat. Commun. **9**, 981 (2018).
[62] M. Parto, S. Wittek, H. Hodaei, G. Harari, M. A. Bandres, J. Ren, M. C. Rechtsman, M. Segev, D. N. Christodoulides, and M. Khajavikhan, Edge-Mode Lasing in 1D Topological Active Arrays, Phys. Rev. Lett. **120**, 113901 (2018).
[63] P. St-Jean, V. Goblot, E. Galopin, A. Lemaître, T. Ozawa, L. Le Gratiet, I. Sagnes, J. Bloch, and A. Amo, Lasing in topological edge states of a one-dimensional lattice, Nat. Photon. **11**, 651 (2017).
[64] M. A. Bandres, S. Wittek, G. Harari, M. Parto, J. Ren,

M. Segev, D. N. Christodoulides, and M. Khajavikhan, Topological insulator laser: Experiments, Science **359**, eaar4005 (2018).
[65] M. Müller, S. Diehl, G. Pupillo, and P. Zoller, Engineered open systems and quantum simulations with atoms and ions, Adv. At. Mol. Opt. Phys. **61**, 1 (2012).
[66] Y. Ashida, S. Furukawa, and M. Ueda, Parity-time-symmetric quantum critical phenomena, Nat. Commun. **8**, 15791 (2017).
[67] H. Shen, and L. Fu, Quantum Oscillation from In-Gap States and a Non-Hermitian Landau Level Problem, Phys. Rev. Lett. **121**, 026403 (2018).
[68] M. Papaj, H. Isobe, and L. Fu, Nodal arc of disordered Dirac fermions and non-Hermitian band theory, Phys. Rev. B **99**, 201107 (2019).
[69] T. Yoshida, R. Peters, and N. Kawakami, Non-Hermitian perspective of the band structure in heavy-fermion systems, Phys. Rev. B **98**, 035141 (2018).
[70] Y. Xu, S.-T. Wang, and L.-M. Duan, Weyl Exceptional Rings in a Three-Dimensional Dissipative Cold Atomic Gas, Phys. Rev. Lett. **118**, 045701 (2017).
[71] J. Li, A. K. Harter, J. Liu, L. de Melo, Y. N. Joglekar, and L. Luo, Observation of parity-time symmetry breaking transitions in a dissipative Floquet system of ultracold atoms, Nat. Commun. **10**, 855 (2019).
[72] S. Lapp, J. Angonga, F. A. An, and B. Gadway, Engineering tunable local loss in a synthetic lattice of momentum states, New J. Phys. **21**, 045006 (2019).
[73] F. K. Kunst, E. Edvardsson, J. C. Budich, and E. J. Bergholtz, Biorthogonal Bulk-Boundary Correspondence in Non-Hermitian Systems, Phys. Rev. Lett. **121**, 026808 (2018).
[74] K. Esaki, M. Sato, K. Hasebe, and M. Kohmoto, Edge states and topological phases in non-Hermitian systems, Phys. Rev. B **84**, 205128 (2011).
[75] T. E. Lee, Anomalous Edge State in a Non-Hermitian Lattice, Phys. Rev. Lett. **116**, 133903 (2016).
[76] A. K. Harter, T. E. Lee, and Y. N. Joglekar, $\mathcal{PT}$-breaking threshold in spatially asymmetric Aubry-André and Harper models: Hidden symmetry and topological states, Phys. Rev. A **93**, 062101 (2016).
[77] S. Yao, F. Song, and Z. Wang, Non-Hermitian Chern Bands, Phys. Rev. Lett. **121**, 136802 (2018).
[78] S. Yao and Z. Wang, Edge States and Topological Invariants of Non-Hermitian Systems, Phys. Rev. Lett. **121**, 086803 (2018).
[79] K. Takata and M. Notomi, Photonic Topological Insulating Phase Induced Solely by Gain and Loss, Phys. Rev. Lett. **121**, 213902 (2018).
[80] Z. Gong, Y. Ashida, K. Kawabata, K. Takasan, S. Higashikawa, and M. Ueda, Topological Phases of Non-Hermitian Systems, Phys. Rev. X **8**, 031079 (2018).
[81] Y. Xiong, Why does bulk boundary correspondence fail in some non-hermitian topological models, J. Phys. Commun. **2**, 035043 (2018).
[82] S. Lieu, Topological phases in the non-Hermitian Su-Schrieffer-Heeger model, Phys. Rev. B **97**, 045106 (2018).
[83] D. Leykam, K. Y. Bliokh, C. Huang, Y. D. Chong, and F. Nori, Edge Modes, Degeneracies, and Topological Numbers in Non-Hermitian Systems, Phys. Rev. Lett. **118**, 040401 (2017).
[84] H. Shen, B. Zhen, and L. Fu, Topological Band Theory for Non-Hermitian Hamiltonians, Phys. Rev. Lett. **120**, 146402 (2018).
[85] H. Zhou, C. Peng, Y. Yoon, C. W. Hsu, K. A. Nelson, L. Fu, J. D. Joannopoulos, M. Soljačić, and B. Zhen, Observation of bulk Fermi arc and polarization half charge from paired exceptional points, Science **359**, 1009 (2018).
[86] A. Cerjan, S. Huang, K. P. Chen, Y. Chong, M. C. Rechtsman, Experimental realization of a Weyl exceptional ring, arXiv:1808.09541 (2018).
[87] K. Kawabata, S. Higashikawa, Z. Gong, Y. Ashida, and M. Ueda, Topological unification of time-reversal and particle-hole symmetries in non-Hermitian physics, Nat. Commun. **10**, 297 (2019).
[88] L. Jin and Z. Song, Bulk-boundary correspondence in a non-Hermitian system in one dimension with chiral inversion symmetry, Phys. Rev. B **99**, 081103 (2019).
[89] C. H. Lee, G. Li, Y. Liu, T. Tai, R. Thomale, and X. Zhang, Tidal surface states as fingerprints of non-Hermitian nodal knot metals, arXiv:1812.02011 (2018).
[90] C. H. Lee, and R. Thomale, Anatomy of skin modes and topology in non-Hermitian systems, Phys. Rev. B **99**, 201103 (2019).
[91] D. S. Borgnia, A. J. Kruchkov, and R.-J. Slager, Non-Hermitian Boundary Modes, arXiv:1902.07217 (2019).
[92] T. Liu, Y.-R. Zhang, Q. Ai, Z. Gong, K. Kawabata, M. Ueda, and F. Nori, Second-Order Topological Phases in Non-Hermitian Systems, Phys. Rev. Lett. **122**, 076801 (2019).
[93] M. Ezawa, Non-Hermitian boundary and interface states in nonreciprocal higher-order topological metals and electrical circuits, Phys. Rev. B **99**, 121411(R) (2019).
[94] M. Ezawa, Non-Hermitian higher-order topological states in nonreciprocal and reciprocal systems with their electric-circuit realization, Phys. Rev. B **99**, 201411(R) (2019).
[95] C. H. Lee, L. Li, and J. Gong, Hybrid higher-order skin-topological modes in non-reciprocal systems, arXiv:1810.11824 (2018).
[96] E. Edvardsson, F. K. Kunst, and E. J. Bergholtz, Non-Hermitian extensions of higher-order topological phases and their biorthogonal bulk-boundary correspondence, Phys. Rev. B **99**, 081302(R) (2019).
[97] See Supplementary Materials for the periodic band structures and more details about the topological invariants and phases, zero flux and chiral symmetric cases, higher-dimensional generalizations, and the experimental realization with references [98, 99].
[98] F. Reiter, and A. S. Sørensen, Effective operator formalism for open quantum systems, Phys. Rev. A **85**, 032111 (2012).
[99] S. Longhi, D. Gatti, and G. D. Valle, Robust Light Transport in Non-Hermitian Photonic Lattices, Sci. Rep. **5**, 13376 (2015).